THE JOURNAL OF BIOLOGICAL CHEMISTRY VOL. 282, NO. 29, pp. 21100–21109, July 20, 2007

C1 Inhibitor Serpin Domain Structure Reveals the Likely Mechanism of Heparin Potentiation and Conformational Disease*[S]

Received for publication, January 29, 2007, and in revised form, April 11, 2007 Published, JBC Papers in Press, May 8, 2007, DOI 10.1074/jbc.M700841200

László Beinrohr[‡1], Veronika Harmat[§¶], József Dobó[‡], Zsolt Lörincz[‡], Péter Gál[‡2], and Péter Závodszky[‡3]

From the [‡]Institute of Enzymology, Biological Research Center, Hungarian Academy of Sciences, Karolina út 29, H-1113 Budapest, Hungary and the [§]Protein Modeling Group and [¶]Laboratory of Structural Chemistry and Biology, Institute of Chemistry, Eötvös Loránd University, Hungarian Academy of Sciences, Pázmány Péter Sétány 1A, H-1117 Budapest, Hungary

C1 inhibitor, a member of the serpin family, is a major down-regulator of inflammatory processes in blood. Genetic deficiency of C1 inhibitor results in hereditary angioedema, a dominantly inheritable, potentially lethal disease. Here we report the first crystal structure of the serpin domain of human C1 inhibitor, representing a previously unreported latent form, which explains functional consequences of several naturally occurring mutations, two of which are discussed in detail. The presented structure displays a novel conformation with a seven-stranded β-sheet A. The unique conformation of the C-terminal six residues suggests its potential role as a barrier in the active-latent transition. On the basis of surface charge pattern, heparin affinity measurements, and docking of a heparin disaccharide, a heparin binding site is proposed in the contact area of the serpin-proteinase encounter complex. We show how polyanions change the activity of the C1 inhibitor by a novel "sandwich" mechanism, explaining earlier reaction kinetic and mutagenesis studies. These results may help to improve therapeutic C1 inhibitor preparations used in the treatment of hereditary angioedema, organ transplant rejection, and heart attack.

C1 inhibitor belongs to the group of serpin-type proteinase inhibitors in blood plasma. Serpins act as pseudosubstrates of serine and cysteine proteinases (although there are noninhibitory serpins as well) (1). A conformational change is triggered in the serpin upon peptide bond cleavage, which distorts the active site of proteinase and traps it in an inactive, covalently linked serpin-enzyme complex (2, 3). Serpins are vital down-regulator components of proteolytic signal amplification cascades. Human C1 inhibitor (C1-inh)[4] is the only inhibitor that acts on early components of the classical pathway (C1r and C1s) and on that of the lectin pathway (MASP-1 and MASP-2) of the complement system (4). Complement mediates host defense against pathogens and altered host cells, but its uncontrolled activation could be harmful. Other physiologically crucial targets include plasma kallikrein and activated factor XII (fXIIa) of the contact activation and activated factor XI (fXIa) of the intrinsic coagulation systems (4). Apart from proteinase inhibition, it was recently discovered that C1-inh binds the central component C3b of complement (5), endotoxins from bacteria (6) and E-, P-selectin adhesion proteins on endothelial cells (7). C1-inh is a single-chain glycoprotein that has atypical two-domain architecture (8) with the C-terminal serpin and the unique N-terminal domains (9). C1-inh is extensively modified post-translationally, bearing six *N*-linked carbohydrates. Sequencing analysis revealed 14 potential *O*-glycosylation sites (9), seven of which had been verified by carbohydrate analysis (10). Most of the sugars are present in the N-terminal domain and do not affect proteinase inhibition (11, 12), but affinity to endotoxins and selectins depends on the *N*-glycans.

The importance of C1-inh is underlined by its deficiency, resulting in hereditary angioedema (HAE) (13). Symptoms of HAE manifest themselves in recurrent tissue swelling, which could be lethal if it occurs in the upper airways. Replacement therapy using C1-inh isolated from human plasma was introduced over 25 years ago (14). Its potential as an anti-inflammatory drug was also apparent. Application of C1-inh was found to be beneficial in ischemia-reperfusion injury (organ transplant rejection, heart attack) and septic shock (15). Recent advances of biotechnology led to the large scale production of recombinant C1-inh from the milk of transgenic rabbits (16).

Activities of many serpins are modulated by ligand binding. The anti-complement activity of heparin, mediated by C1-inh, was recognized decades ago (17), but the mechanism is still unclear (4, 18). Heparin is a naturally occurring sulfated

* This work was supported by the European Community-Research Infrastructure Action under the FP6 "Structuring the European Research Area Programme" contract RII3-CT-2004–506008; Hungarian Ministry of Health Grant ETT; Hungarian National Science Foundation (OTKA) Grants T046444, T096912, D42199, and NI-61915; and the János Bolyai postdoctoral fellowship (to Z. L.). The costs of publication of this article were defrayed in part by the payment of page charges. This article must therefore be hereby marked "*advertisement*" in accordance with 18 U.S.C. Section 1734 solely to indicate this fact.

[S] The on-line version of this article (available at http://www.jbc.org) contains supplemental Tables S1 and S2 and Figs. S1–S4.

The atomic coordinates and structure factors (code 2OAY) have been deposited in the Protein Data Bank, Research Collaboratory for Structural Bioinformatics, Rutgers University, New Brunswick, NJ (http://www.rcsb.org/).

[1] To whom correspondence may be addressed. Tel.: 36-1-209-3535; Fax: 36-1-466-5465; E-mail: lbeinrohr@enzim.hu.

[2] To whom correspondence may be addressed. Tel.: 36-1-209-3535; Fax: 36-1-466-5465; E-mail: gal@enzim.hu.

[3] To whom correspondence may be addressed. Tel.: 36-1-209-3535; Fax: 36-1-466-5465; E-mail: zxp@enzim.hu.

[4] The abbreviations used are: C1-inh, C1 inhibitor; rC1-inh, recombinant C1 inhibitor; HAE, hereditary angioedema; GAG, glycosaminoglycan; RCL, reactive center loop; MOPS, 3-(*N*-morpholino)propanesulfonic acid; fXIIa and fXIa, factor XIIa and XIa, respectively.

polysaccharide (glycosaminoglycan (GAG)). The widely used anticoagulant therapy is based on the prototype of GAG-protein interactions, where a heparin chain binds both the serpin antithrombin and the proteinase thrombin. Heparin works as a template; it speeds up the formation of the Michaelis complex and stabilizes it by bridging the two proteins (19, 20). Allostery also plays an important role in the heparin activation of antithrombin (21) and heparin cofactor II (22). These mechanisms fail to explain the effect of GAGs on C1-inh. We determined the structure of N-terminally truncated human C1-inh to understand how heparin and related polyanions alter its activity.

EXPERIMENTAL PROCEDURES

Protein Expression and Purification—The cDNA clone of human C1-inh (allele V458M) was kindly provided by Susan Clark Bock (9). The EcoRI restriction site was eliminated from the gene. The construct of truncated recombinant C1-inh (rC1-inh) contained six histidines at the N terminus followed by residues Thr^{97}–Ala^{478} (Fig. 1*A*). The DNA construct was ligated into pPic9K vector (Invitrogen) between SnaBI and EcoRI sites. The *Pichia pastoris* GS115 strain (Invitrogen) was transformed with the DraI-digested plasmid, and then His^+ Mut^S clones were isolated. Expression was conducted in a fermentor with a 2-liter vessel (Biostat B; B. Braun). A 40-ml starter culture was grown for 2 days in yeast peptone dextrose medium (Invitrogen). The fermentor was loaded with a 1.5-liter medium of 1% (w/v) yeast extract, 2% (w/v) peptone, 1× yeast nitrogen base (Invitrogen), 0.1 M KH_2PO_4, 4% (v/v) glycerol and inoculated with the starter. After depletion of batch glycerol, the cells were fed with 50% (v/v) glycerol, and the culture was grown until the wet cell weight reached 200 g $liter^{-1}$. Recombinant C1-inh production was induced with 25% (v/v) methanol and 40% (w/v) sorbitol for 2–3 days. The pH was kept at 6.0 with NH_3, the temperature was kept at 25 °C, and phenylmethylsulfonyl fluoride (0.2 mM final concentration) was added twice daily during the induction period. Phenylmethylsulfonyl fluoride and EDTA were added to the clarified supernatant to a final concentration of 0.5 and 25 mM, respectively, and then stored at −70 °C until use. Nickel affinity purification of recombinant C1-inh was performed (Ni^{2+}-nitrilotriacetic acid Superflow; Qiagen). Cation exchange chromatography followed (Source 15S column; GE Healthcare), using a 10-column volume 0–0.5 M NaCl gradient in the following buffer: 20 mM MOPS, 0.1 mM EDTA, pH 7.0. Active and latent rC1-inh forms were separated at this step. The purified proteins were deglycosylated at 4 °C using endoglycosidase H (New England Biolabs) for 1 week. The deglycosylated protein was purified again by cation exchange as above, followed by gel filtration (Sephadex 75 HiLoad 16/60; GE Healthcare). The purified recombinant C1-inh was concentrated to 10–14 mg ml^{-1}. Protein concentration was estimated from the absorbance of the solution at 280 nm using the extinction coefficient of 0.64 ml mg^{-1} cm^{-1}, calculated from the protein sequence using the Expasy ProtParam tool.

Deglycosylation of Recombinant C1-inh—4.6 μg of glycosylated active recombinant C1-inh (in 10 μl) was used to demonstrate heterogeneity caused by *N*-glycans. Samples were incubated at 37 °C for 1.5 h, with or without 100 units of endoglycosidase H. β-Mercaptoethanol reduced and nonreduced samples were run on 12.5% SDS-PAGE (Fig. 1*B*).

Activity Test of C1-inh Forms—The reactivity of different C1-inh forms was tested with target proteinase C1s and nontarget proteinase trypsin. 0.4 μg of activated C1s (Calbiochem) in 10 μl was used throughout. Bovine pancreatic trypsin (T-1426; Sigma) was dissolved and dialyzed in 1 mM HCl, and then 0.2 μg (in 1 μl) was used in all reactions. Three forms of C1-inh were tested. 2.3 μg of lyophilized plasma C1-inh (Berinert P; ZLB Behring), 2.8 μg of active deglycosylated recombinant C1-inh, and 7.4 μg of latent deglycosylated recombinant C1-inh was made up to 5 μl with buffer containing 140 mM NaCl, 20 mM HEPES, 0.1 mM EDTA, pH 7.4, and used in a reaction. Reaction mixtures were incubated at 37 °C for 1 h and analyzed on 12.5% SDS-PAGE (Fig. 1*C*). The specific activity of recombinant C1-inh was probed with excess C1s under conditions identical to those described above. ~9 μg of C1s was reacted with 0.31, 0.63, 1.25, and 2.5 μg of active deglycosylated recombinant C1-inh (in a 10-μl volume). Over 90% of the protein was reactive toward C1s, and ~70% formed a covalent complex (Fig. S1).

Thermal Stability Measurements of C1-inh Forms—Dilutions with 140 mM NaCl, 20 mM HEPES, 0.1 mM EDTA, pH 7.4, buffer were made to yield 0.1–0.2 mg ml^{-1} C1-inh solutions. Differential scanning calorimetry scans were recorded using VP-differential scanning calorimetry (MicroCal) in the range of 30–125 °C, at a rate of 1 °C min^{-1}, with 15-min preincubation at 30 °C and a 2–4-s data accumulation time. Buffer was used as reference. Melting temperatures were read at peak maximas. The results are summarized in Table 1.

Crystallization and Structure Determination of Latent Recombinant C1-inh—Crystallization trials were set up using the hanging drop method at 20–25 °C, 2–4-μl drops with a protein/reservoir solution ratio of 1:1. Crystals grew in condition 35 (Crystal Screen I; Hampton Research) within 2 weeks. The crystals were cryoprotected by soaking in reservoir solution containing 20% (v/v) glycerol. Collections of diffraction data were carried out at 100 K on beamline X11 of the EMBL outstation at DESY (Hamburg, Germany) (wavelength 0.8162 Å). The asymmetric unit contained one molecule. Data were processed using the XDS package (23). The structure was solved by molecular replacement using MOLREP of the CCP4 package (24). Molecular replacement using structures of individual serpins failed, so a superimposed structure ensemble of various serpins was used as a search model. The following structures were acquired from the Protein Data Bank, quoted with respective Protein Data Bank codes: 4CAA, 1QMB, 1E05, 1DVN, 1C8O, 1JTI, 1JJO, 1MTP, 1HLE, and 1JRR. Structurally nonconserved regions, N terminus, and the reactive center loop (RCL) were removed from the search model of molecular replacement using DeepView (25). Refinement was carried out with the REFMAC5 program, using TLS refinement and restrained maximum likelihood refinement (26). Manual model building was carried out using the program COOT (27). Residues of the N and C terminus, three short disordered segments, and side chains of some surface residues were not built in the model due to a lack of electron density. The final model contains residues 101–102, 105–137, 142–293, and

296–476, one covalently bound saccharide, three glycerol, and 70 water molecules. 90.4 and 9.6% of the residues are in the most favored and additional favored regions of the Ramachandran plot, respectively. Data collection and refinement statistics are summarized in Table 2.

Polymerization Tendency of C1-inh Forms—See supplemental materials and Fig. S2.

Heparin Affinity Measurements of C1-inh Forms—Heparin affinity chromatography was performed on a 1-ml column (HiTrap Heparin HP; GE Healthcare) in a buffer containing 20 mM HEPES, 0.1 mM EDTA, pH 7.4. 30–300 μg of C1-inh in a 200-μl volume was injected and washed extensively with buffer, and then a linear salt gradient of 0.0–0.5 M NaCl in a 15-ml volume was applied to elute proteins. Absorbance at 280 nm and conductivity were monitored continuously during the gradient (ÄKTApurifier; GE Healthcare) (Fig. 4).

Modeling—The structures of the serpins latent α_1-proteinase inhibitor (28) (1IZ2), cleaved protein C inhibitor (29) (1LQ8), and dimeric antithrombin (30) (1E04) were obtained from the Protein Data Bank. The structures of proteinases fXIa (31) (1XX9), C1s (32) (1ELV), plasma kallikrein (33) (2ANW), MASP-2 (34) (1Q3X), and C1r (35) (1MD8) were used. MASP-1 and fXIIa were modeled using SWISS-MODEL (25). Glycans were added using the GlyProt server (36). All proteinases were truncated to the beginning of the activation peptide, so only the catalytic serine proteinase domains were retained. Electrostatics was calculated using APBS (37) and PDB2PQR. Crystal contacts were evaluated using PISA (38).

Blind Docking—The structure diagram and the released torsion angles of the docked heparin disaccharide are depicted in Fig. 5*C*, derived from protein-saccharide complex structures 1T8U and 1XMN. Residue pairs SGN2-IDS3 in Protein Data Bank entry 1T8U and SGN4-IDS5 of chain U in Protein Data Bank entry 1XMN were taken as models of the disaccharide in twist-boat and chair conformations, respectively. Initial calculations with both models yielded similar docked ensembles, so further calculations were carried out with saccharide rings in chair conformation. Calculations were carried out on our C1-inh crystal structure (Protein Data Bank code 2OAY). Active antithrombin both in heparin-bound (39) (1AZX) and -free conformations (1E04) were also used for method validation. The macromolecules were prealigned using AMoRe of the CCP4 suite. Structures were prepared for docking in AutoDockTools; polar hydrogen atoms were added to the structures, and Gasteiger and Kollman united atom charges were used for the ligand and protein atoms, respectively. First docking was carried out on the whole protein represented with coarse grid maps ($100 \times 96 \times 86$ grid points with 1.0-Å spacing). The best solution was used for further docking with fine grid maps ($108 \times 108 \times 108$ grid points with 0.375-Å spacing). AutoGrid and AutoDock were used for calculation of grid maps and docking, respectively (using the Lamarckian Genetic Algorithm) (40). Docking was carried out with default parameters. The number of trials was set to 100, with an initial population of 250 individuals, 2×10^7 energy evaluations, and 27,000 generations. The resulting docked structures were clustered with 3- and 1-Å root mean square deviation tolerances for the first and second docking runs.

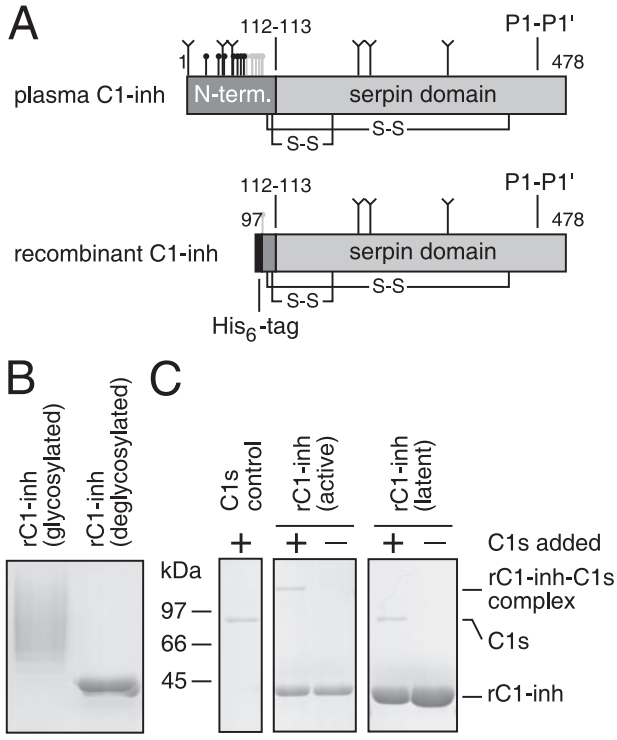

FIGURE 1. **Structural features, electrophoretic mobility, and activity of C1-inh forms.** *A*, schematic representation of the two-domain structure of C1-inh and the recombinant construct used in our study. Residue numbering conforms to the mature protein, and post-translational modifications are shown as they appear in primary sequence (9). *v-shaped symbols*, *N*-glycans; *black circles*, *O*-glycans; *gray circles*, probable *O*-glycans. *S–S*, disulfide linkages. *B*, nickel affinity purified rC1-inh from yeast appears smeared between 50 and 100 kDa on SDS-PAGE. Deglycosylation with glycosidase enzyme produces protein with the expected size, migrating as a single band at ~44 kDa. *C*, activity of rC1-inh forms were tested *in vitro*, and reaction mixtures were visualized on SDS-PAGE. C1-inh forms (rC1-inh active and rC1-inh latent) were incubated with the target proteinase C1s. Inhibition by a serpin mechanism results in formation of SDS-resistant serpin-proteinase complexes. The results demonstrate that active rC1-inh forms a covalent complex with C1s. In contrast, latent rC1-inh leaves C1s intact. The complete version of this panel is available as supplemental Fig. S1.

Visualization—Figures were prepared using PyMOL (DeLano Scientific). Additional figures were produced with InkScape, CS ChemDraw Pro (CambridgeSoft), and Origin (MicroCal).

RESULTS

Expression and Structure Determination—A C1-inh serpin domain construct (in which the first 96 amino acids of the wild-type protein were replaced with a His-tag) was engineered to reduce heterogeneity and to aid purification. This truncation removes the nonconserved part of C1-inh and leaves most of the biological activities essentially unchanged (11, 12) (Fig. 1*A*). The truncated rC1-inh, expressed in *P. pastoris*, was visualized as a smear between 50 and 100 kDa on SDS-PAGE, since it was heterogeneously glycosylated (Fig. 1*B*). Purification yielded two forms; one formed a covalent complex with C1s, and the other did not (Fig. 1*C*). *N*-Glycans were removed enzymatically, resulting in a homogeneous protein migrating at ~44 kDa. Differential scanning calorimetry measurement of the inactive form showed a melting temperature between that of the active and cleaved rC1-inh forms (Table 1). The noninhibitory form

TABLE 1
Melting temperatures of C1-inh forms

C1-inh form	Active	Latent	Cleaved
Plasma C1-inh	60.0 °C	ND[a]	115.6 °C
rC1-inh (glycosylated)	53.8 °C	ND[a]	114.8 °C
rC1-inh (deglycosylated)	54.0 °C	69.0 °C	ND[a]

[a] ND, not determined.

was crystallized, and a full data set was collected. The structure was determined using molecular replacement and refined to 2.35 Å resolution (Table 2).

Overall Structure—Our structure represents the serpin domain (residues 113–478) and a small portion of the N-terminal domain (residues 97–112). The overall structure of rC1-inh resembles those of other serpins (1), with highly conserved nine α-helices and three β-sheets present (Fig. 2*A*). The His-tag is not observed, and the remaining part of the unique N-terminal domain is poorly ordered. This small portion of the N-terminal domain is anchored with two nonconserved disulfide bonds along the D and E helices. Structural alignment with other serpin structures reveals major differences at helix D and the loop connecting it with the second strand of sheet A (s2A), where the helix is shortened to 2 turns and s2A is shortened by 2 residues (Fig. 2, *A* and *B*). The uncleaved RCL is incorporated into sheet A, forming s4A. Insertion occurred up to position P5, where P1-P1′ denotes the Arg^{444}-Thr^{445} scissile bond (Fig. 3*A*). This classifies the crystallized form of rC1-inh as latent (41). A well defined hydrogen bonding network and burial of reactive center residues explain the loss of inhibitory activity. A striking feature of our structure is that the C-terminal P′ part of the RCL forms the new seventh strand of sheet A, making it a fully antiparallel β-sheet (Figs. 2*A* and 3*A*). This segment forms a flexible surface loop in all other known latent serpin structures (28, 41, 42). Apart from backbone strand-strand interactions, hydrogen bonds with the side chains of Gln^{385} and Gln^{420} stabilize its conformation. The conformation of the nearby C-terminal tail (encompassing the last 6 residues of the protein) is also unique to rC1-inh. The conformation of this tail is conserved in known serpin structures (1, 43), since the C_α positions of the highly conserved Pro^{391} of α_1-proteinase inhibitor and equivalent prolines in other structures deviate no more than 3 Å (Fig. 3*C*). In other serpins, the C-terminal tail is placed to the side of strand s6A in sheet A. In contrast, this segment of rC1-inh is folded in a topologically unique way. It is on the other side of the RCL, and the conserved Pro^{476} is moved away by more than 10 Å (Fig. 3*B*) compared with the position found in other serpins (Fig. 3*C*). This conformational change can solely be attributed to a rigid body rotation of backbone around Tyr^{474}, whose Ψ angle made an almost complete turn of ~180°.

Crystal Contacts Suggest the Existence of a New Type of Polymeric C1-inh—The loop connecting helix I with s5A displays an unusual conformation. Phe^{396} and Phe^{397} residues are exposed, whereas charged Glu^{395} and Asp^{398} are turned inside. This loop is embedded in a hydrophobic groove of another molecule, forming a crystal contact (Fig. S2). The groove is formed by the peeling of strand s1C during latency transition in serpins. The rC1-inh contact interface is mainly hydrophobic in nature, with a total buried accessible surface area of ~2100 $Å^2$ (Table S1).

TABLE 2
Data and refinement statistics

Parameter	Value
Data collection	
Space group	$P6_5$
Cell dimensions	
a, *b*, *c* (Å)	98.90, 98.90, 94.68
α, β, γ (degrees)	90.00, 90.00, 120.00
Resolution (Å)[a]	20.0-2.35 (2.40-2.35)
R_{merge}[a]	0.097 (0.652)
$I/\sigma I$[a]	20.29 (3.89)
Completeness (%)[a]	99.8 (100.0)
No. of reflections	
Observed reflections[a]	319,446 (12,799)
Unique reflections[a]	21,930 (1,341)
Refinement	
Resolution (Å)	20.0-2.35
R_{work}/R_{free}[b]	0.174/0.218
No. of atoms	
Protein	2,858
Saccharide and glycerol	32
Water	70
B factors	
Protein	34.20
Saccharide and glycerol	69.98
Water	52.79
Root mean square deviations	
Bond lengths (Å)	0.020
Bond angles (degrees)	1.76

[a] Values are in parentheses for the highest resolution shell.
[b] 5.1% of the reflections were in a test set for monitoring the refinement process.

Through this atypical interface, latent rC1-inh molecules form novel type, linear polymers in the crystal with a 3-fold screw symmetry. Theoretically, this linkage could also persist between one latent molecule and one other C1-inh form, so involvement in C1-inh deficiency was suspected (44). Nondenaturing PAGE and gel filtration were employed to check whether polymers form out of latent rC1-inh molecules *in vitro*. Latent rC1-inh was eluted as a single peak consistent with the monomeric form upon gel filtration in physiological buffer (data not shown). Incubation at different temperatures was performed in buffers with pH 5.0 and 7.4. Active rC1-inh polymerizes under these conditions, but the majority of latent rC1-inh remains still homogeneous on PAGE. The addition of glycerol promoted the appearance of a higher molecular mass band, compatible with dimer formation (Fig. S3).

RCL Insertion Increases Heparin Affinity—Our presumption was that a change in heparin affinity upon RCL insertion or glycan removal could help localize the heparin binding site. Heparin binding of different C1-inh forms was probed with heparin affinity chromatography. Plasma and recombinant C1-inh forms (active, RCL-cleaved, and latent variants) were studied. Both the cleaved and the latent forms have the RCL inserted into β-sheet A; however, the latter has an intact RCL. All cleaved forms exhibited higher affinity to heparin than active counterparts (Fig. 4) irrespective of their origin. Latent and cleaved forms had similar affinity. Deglycosylation also increased affinity, and the effects of cleavage and deglycosylation were additive. In summary, RCL insertion results in increased affinity to heparin. This effect is different from that observed in other heparin-activable serpins (30). Similar chromatograms were obtained using a strong cation exchanger (data not shown), indicating a nonspecific ionic interaction site close to the RCL in active C1-inh.

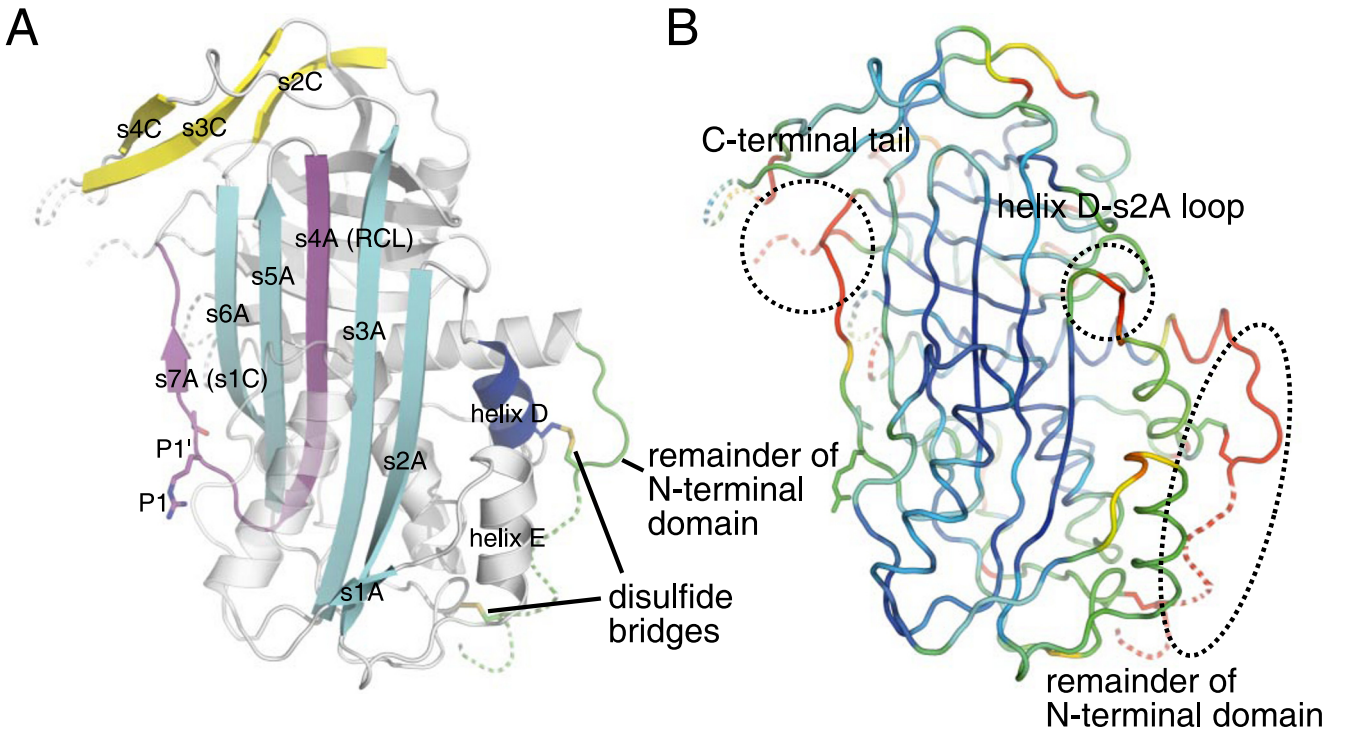

FIGURE 2. **Overall structure of latent rC1-inh serpin domain.** *A*, view of rC1-inh in cartoon diagram representation. Latent rC1-inh has the largest β-sheet A among serpins with seven β-strands (*colored cyan* and *magenta*). The RCL (*colored magenta*) and even the s1C segments are tightly embedded in sheet A. Burial of RCL residues explains the loss of inhibitory activity. Labeling of secondary structure elements follows conventions (1). Residues not observed in the structure are shown *dashed*. Disulfide bridges and P1 and P1′ residues are shown as *sticks*. *P1-P1′*, Arg^{444}-Thr^{445} reactive bond. *B*, root mean square deviation *colored ribbon representation* of rC1-inh. Backbone atoms of latent rC1-inh were superimposed to the latent α_1-proteinase inhibitor structure. *Coloring* from *red* to *blue* indicates residues from most deviating to most similar. The most differing regions (*dashed circles*) include the unique N-terminal domain, helix D, and the C-terminal tail (the last 6 residues) of rC1-inh.

Charge Distribution and Docking Suggest a Heparin Binding Site at the Enzyme-Inhibitor Interface— The interaction between negatively charged GAGs and positively charged regions in proteins allows identification of possible binding sites based on electrostatics (29) (Fig. S4). Examination of the electric field of latent rC1-inh revealed an almost symmetric bipolar charge distribution. A positive electric field protrudes from the "top" of the serpin, whereas a negative one protrudes from the "bottom" (Fig. 5*A*). Mapping the field onto the solvent-accessible surface revealed a single contiguous positive region of 35 Å diameter crowning strands s2C and s3C and the loop connecting s3A with s4C (Fig. 5*B*). Other contributing elements include s4C and surface segments of sheet B (strands s4B, s5B, and s6B). Based on structural homology with other serpins, the RCL in active rC1-inh happens to span this patch (1, 43). Displacement of the neutral RCL in the cleaved and latent forms predictably diminishes steric hindrance, increasing accessibility to heparin, consistent with the affinity measurements. Furthermore, this region vastly overlaps with the area, where the proteinase docks to form the initial noncovalent Michaelis complex (19–22). Smaller positively charged patches were also identified in the proximity of helix F and the C-terminal side of s2A. Further inspection showed that *N*-glycans shield these outlying patches (Fig. S4). In order to verify the GAG binding site, we carried out blind docking studies. A heparin disaccharide was used as ligand (Fig. 5*C*), and no prior assumption was made on binding sites. The same method was used to dock the ligand on active antithrombin, which was chosen as a reference to validate the method on our system. Docking on latent rC1-inh resulted in two overlapping binding sites both being on the large positively charged region (Fig. 5*D*). The charged residues in the first site contributing to ligand binding are Lys^{278}, Lys^{306}, Lys^{307}, and Lys^{368}. The second site is more extended and partially contains the first site and residues Lys^{284}, Lys^{285}, and Arg^{287} (Table S2). It was shown earlier by mutation experiments that Lys^{284} and Arg^{287} contribute to heparin activation of C1-inh (18). The disaccharide did dock to the same site in several different orientations, indicating nonspecific binding. We suppose that longer heparin chains would simultaneously bind to both binding sites.

Charge Distribution of Target Proteinases Suggests a Neutralization Mechanism of C1-inh Potentiation—The only major positively charged patch on rC1-inh can be found at the presumed enzyme-inhibitor interface (Fig. 5, *A* and *B*). Presumably, polyanions bind this area during inhibition, neutralizing positive charges or even providing excess negative ones. In this way, polyanions get "sandwiched" between the inhibitor and the enzyme. Based on this assumption, we must be able to predict which C1-inh-proteinase reaction is accelerated or slowed by polyanions. We compared the surface charges of target proteinases to test this "sandwich" mechanism. To make results comparable, we visualized the active site cleft and specificity loops of the serine proteinase domains. C1s, plasma kallikrein, fXIa, and fXIIa were included in the study, since independent experimental data were available in the literature. Polyanions increase inhibitory capacity against fXIa the most (60–115-fold

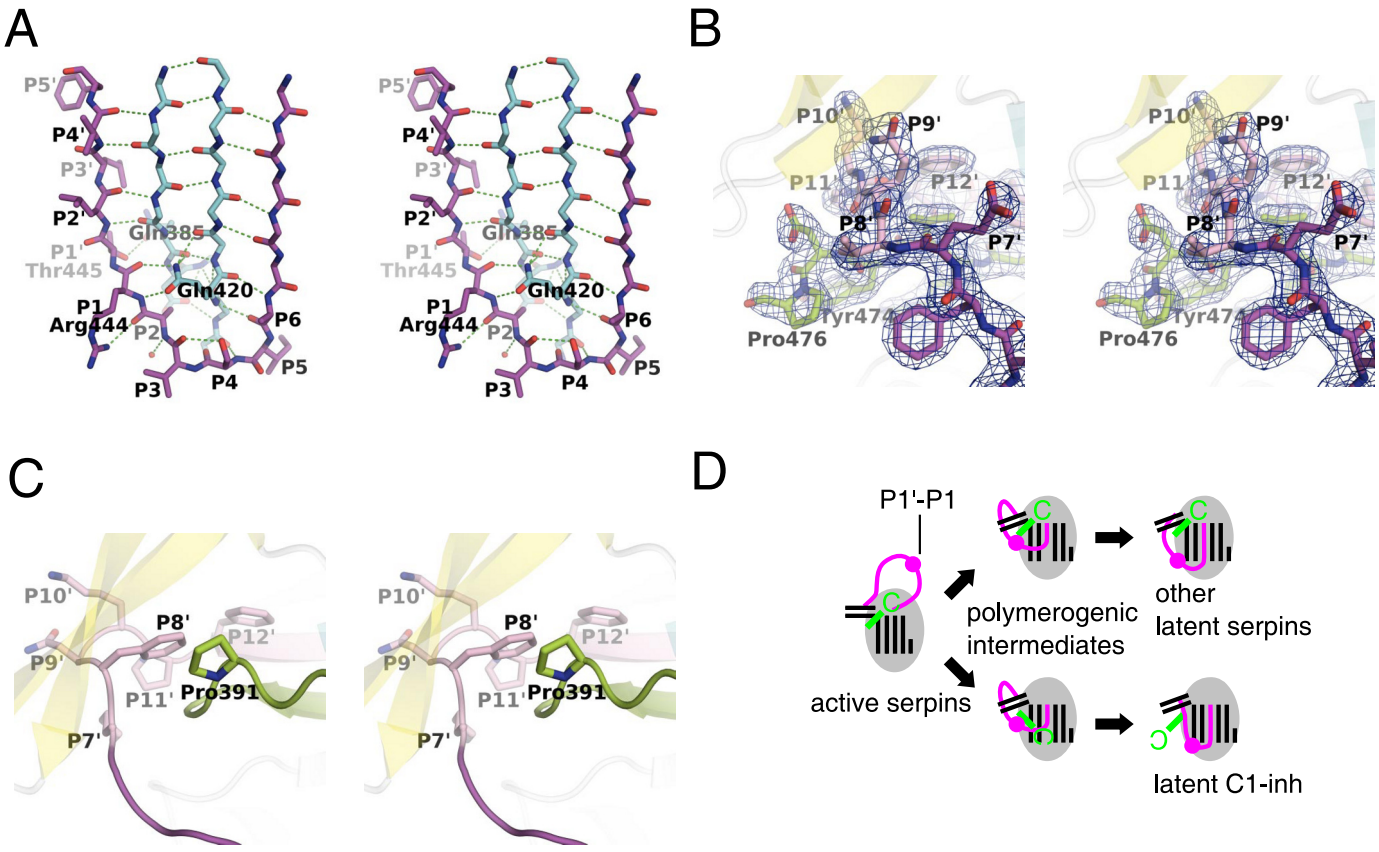

FIGURE 3. **Novel interactions in latent rC1-inh structure.** *A*, stereo view of sheet A of rC1-inh (*cyan* and *magenta strands*) and its extended hydrogen bond network stabilizing the entire RCL (*magenta*). *B*, stereo view of the C-terminal tail with electron density map contoured at the 1.0 σ level. The tail (*green*) differs not only in the position but also in the way it is folded around the RCL (*magenta*). *C*, stereo view of the C-terminal tail of latent α_1-proteinase inhibitor. Orientation and coloring is the same as in *B*, to make the images comparable. Note that the conserved position of Pro^{391} is occupied with P7′-P8′ RCL residues in rC1-inh instead of the equivalent Pro^{476}. *D*, schematic drawing of the hypothetical mechanism of active-latent transition. Latent serpins have their sheet A extended, where the RCL (*magenta*) inserts in sheet A without RCL cleavage. Strands of sheet C (depicted here as the two-stranded sheet) tilt to allow the RCL to pass, deduced from latent structures known so far (*top row*). Sheet A is seven-stranded in rC1-inh, since the entire RCL is inserted, forming two new strands (*bottom row*). This imposes a steric clash with the conserved C terminus (*green*) if left unaltered. Latency transition is probably enabled through rotated gating of the C terminus.

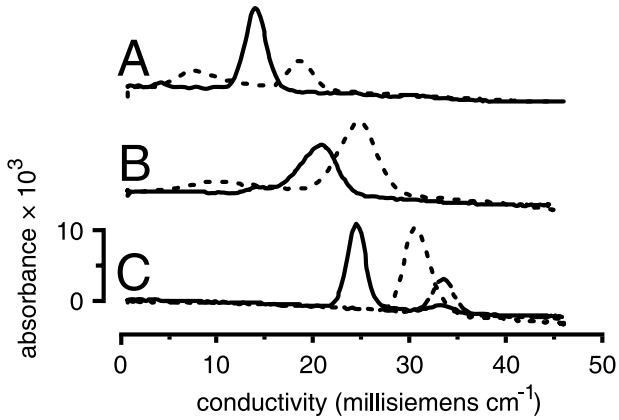

FIGURE 4. **Heparin affinities of different C1-inh forms were compared using heparin affinity chromatography.** *A*, glycosylated, active plasma C1-inh displays the lowest affinity to heparin (*solid line*). Upon RCL cleavage, the affinity increases (*dashed line*). Heparin affinity of plasma C1-inh also increases after treatment with neuraminidase, which removes the negatively charged carbohydrate sialic acid from glycans (data not shown). *B*, glycosylated active rC1-inh binds heparin more strongly (*solid line*), partly due to a lack of negatively charged carbohydrates absent in proteins derived from *Pichia*. The affinity increase upon RCL cleavage (*dashed line*) is similar to that of the plasma protein. *C*, enzymatically deglycosylated active rC1-inh (*solid line*) has the highest affinity to heparin among the active forms. Affinity increase upon RCL cleavage is observed (*dashed line*) as in the cases of plasma and glycosylated recombinant C1-inh. The affinity of latent deglycosylated rC1-inh (*dashed and dotted line*) to heparin is similar but is somewhat higher than that of the cleaved form.

potentiation) (45, 46), followed by C1s (15–60-fold) (47, 48), and a minor effect is observed on plasma kallikrein (~2-fold increase) (49). In contrast, the reaction against fXIIa is hindered 2–4-fold (45). Potentiation factors of these reactions correlate well with the estimated positive charge present on the contact site (Fig. 5*B*). Indeed, fXIa carries the most positive charges, and polyanions have the most significant effect here. Plasma kallikrein has less charged basic patches and extended acidic ones. Inhibition of fXIIa is slowed by polyanions, in accordance with the fact that fXIIa is strikingly acidic. For C1r, MASP-1, and MASP-2, limited data are available, but it is known that potentiation against C1r is at least 5-fold lower than for C1s (47), in agreement with the extended acidic stretches in C1r (Fig. S4).

DISCUSSION

Engineering recombinant C1-inh, adjustment of microbial fermentation conditions, and enzymatic removal of glycans were decisive factors in our success in determining the structure of C1-inh. Our structure represents the so-called latent form, an inactive serpin conformation without RCL cleavage (28, 41, 42). Earlier observations indicated the existence of a monomeric, loop-inserted uncleaved form of heat-treated plasma C1-inh (44). Additionally, the dominant form of some mutant C1-inh variants also displayed an intermediate heat sta-

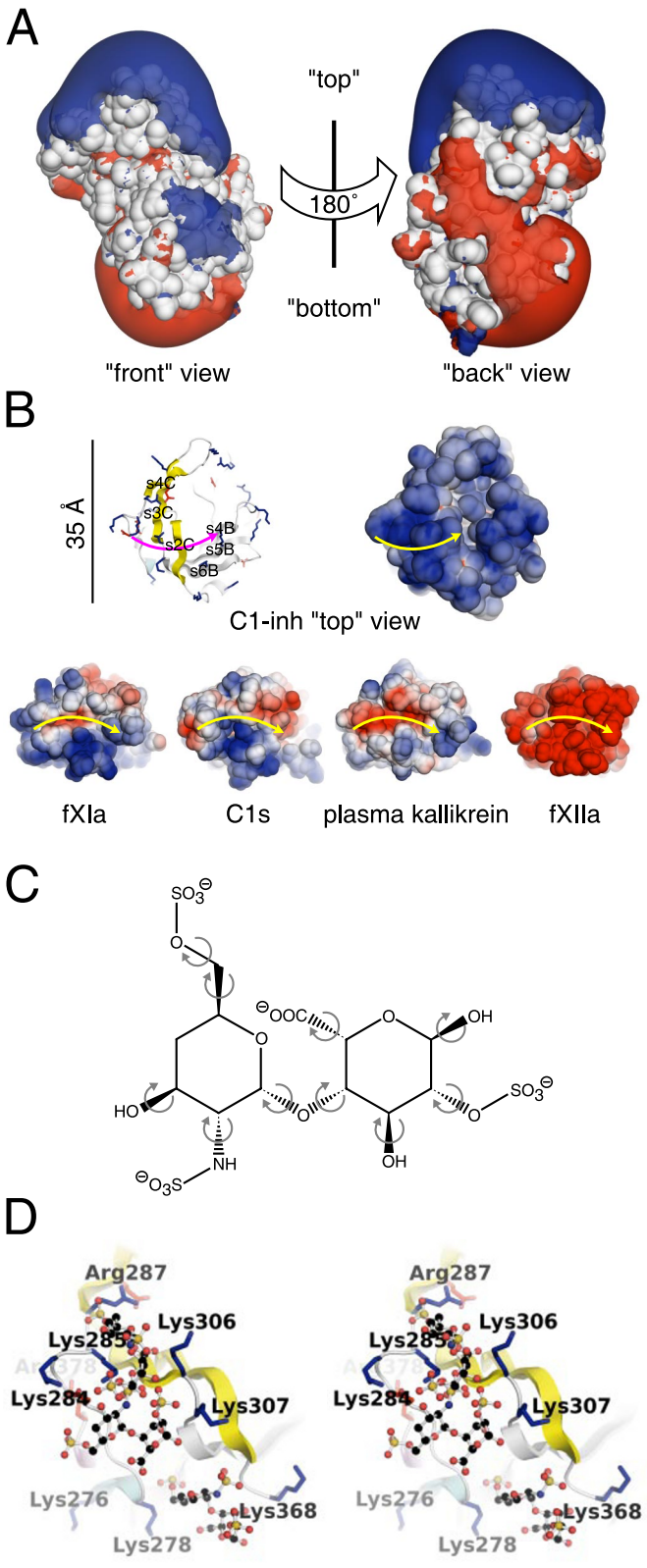

FIGURE 5. **Charge pattern of contact surfaces on enzyme and inhibitor suggests neutralization by polyanions.** *A*, electrostatic potential of latent rC1-inh is bipolar, computed from the crystal structure. *Blue*, positive field; *red*, negative field. *B*, surface charge distribution at the contact surfaces of target proteinases and C1-inh in the predicted encounter complex. The surface representation is *colored* according to the electric field: *blue* is positive, and *red* is negative. *Yellow arrows* indicate the presumed position of the RCL in the Michaelis complex. In the *ribbon diagram* showing the contact site on latent rC1-inh, charged residues appear as sticks and are *colored blue* for positive and *red* for negative. Here, the RCL is shown as a *magenta arrow*. The top of latent rC1-inh is uniformly positive. The four best characterized proteinases are shown. The larger the positive regions around the substrate-binding cleft are, the more effective the activation caused by the polyanions is. For fXIIa, polyanions decrease the reaction rate, which is in line with its negative surface. *C*, structure diagram of the heparin disaccharide used in the blind docking experiments. Bonds rotatable are marked with *gray arrows*. The four ionized sulfate and carboxylate groups are shown with *charge signs*. *D*, docking of a heparin disaccharide (*ball and stick*) reveals a nonlinear heparin binding site. A representative ensemble of docked structures is shown. Charged residues on latent rC1-inh are shown as *sticks*. Arg^{378}, Arg^{287}, and Lys^{284} were previously identified as heparin binding residues (18).

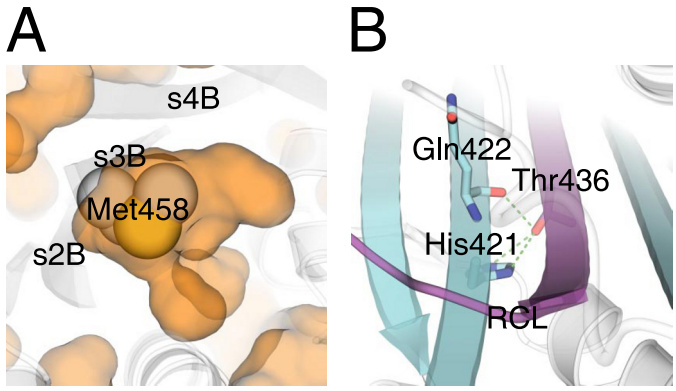

FIGURE 6. **Showcase of mutations.** *A*, studies failed to detect any effect of the V458M polymorphism, although the conserved hydrophobic core (around strands s2B, s3B, and s4B) is involved (53). The reason is that the side chain of Met^{458} (*space-filled*) sits in the biggest cavity of rC1-inh (*orange cloud*); hence, spatial differences are tolerated. *B*, the A436T mutation affects a residue whose side chain becomes buried upon RCL incorporation. Similar mutants of other serpins usually result in cleavable noninhibitory serpins, because loop insertion is hindered. Unexpectedly, the A436T mutant C1-inh is found predominantly in noncleavable loop-inserted forms (51). In the modeled mutant structure, the side chain of Thr^{436} forms a novel hydrogen bond network with the side chain of His^{421} and the backbone of Gln^{422}. This makes the RCL-inserted protein more stable.

bility falling between that of the active and cleaved form (50, 51). However, currently there is no evidence for the occurrence of latent native C1-inh in human plasma. Our structure provides the first direct evidence showing the intact RCL inserted into sheet A in the case of C1-inh (Fig. 2*A*). Relatively low protein concentration, lower than physiological pH in *Pichia* culture, and prolonged storage seemed to promote latency, reaching as much as 30% of total C1-inh.

Over 150 mutations of the C1-inh gene associated with HAE were described and published in a public data base (HAEdb) (52). The effect of frameshifts, large deletions, and insertions can be readily explained. Our structure can be useful in explaining the consequences of point mutations (about 50 cases). We selected two of them on the basis that the mutant proteins had been experimentally characterized and that results could not be explained by serpin homology. The common polymorphism V458M affects 30% of people. Studies failed to detect any effect of this mutation (53), although the conserved hydrophobic sheet B is involved. This residue is found in a large cavity inside the protein, which explains why this steric change does not disrupt internal packing (Fig. 6*A*). The A436T mutation affects a residue whose side chain becomes buried upon RCL incorporation. Unlike similar mutants of other serpins, this mutant is not cleavable by proteinases (51). From the structure, it is evident that the mutant residue packs even better in the loop-

inserted rC1-inh than the wild type residue (Fig. 6*B*), which explains its observed preference for the more stable latent conformation.

Unexpected structural features of latent rC1-inh give the opportunity to derive new information about serpin polymerization and serpin metastability. The unusual conformation of certain side chains, where polar residues are buried and hydrophobic ones seem exposed, focused our attention on the crystal contact involving sheet C and a surface loop (Fig. S2). The possibility of polymer formation with a new topology is tempting. Once thought nonspecific aggregation, serpin polymerization is now regarded as a specific process, causing the majority of serpin-related diseases. Polymer chains vary in length and linkage, which prevents elucidation of the mechanism of their formation at the atomic level (44). Even supposed crystal contacts were found valuable. A similar interaction was first seen in crystals of active-latent dimeric antithrombin (42) and proven later to be physiologically significant (54). However, under the examined conditions, latent rC1-inh is less prone to polymerization than active rC1-inh; thus, the relevance of the observed contact is uncertain.

The second unexpected structural feature of latent rC1-inh is the location of the conserved C-terminal tail (Fig. 3*B*), along with the presence of a new β-strand of sheet A. In all other serpin structures, including latent, RCL-cleaved, and active ones, with the exception of latent plasminogen activator inhibitor-1, the highly conserved proline residue close to the C terminus is found in almost exactly the same position (43) (Fig. 3*C*). One might speculate that there is a connection between the unusual conformation (position of the C terminus and the presence of the seventh β-strand) and the active-to-latent transition and polymerization. It is possible that the C terminus acts as a barrier to RCL insertion, since it needs to relocate compared with its presumed position in active C1-inh, to make room for the upcoming portion of the RCL seen in our latent structure. Thus, an alternative, "gating" mechanism is proposed for the formation of latent C1-inh, which is in line with the observed structural features and explains the effect of frequent C-terminal substitutions (Fig. 3*D*). Indeed, the P476S mutation in C1-inh promoted the formation of a presumably latent variant and polymers (50).

The primary determinant of serpin specificity and reaction rate is the flexible reactive center loop (1, 55). Its sequence, notably the P1 residue, matches the specificity of the target proteinases. Cleavage in the RCL at other residue results normally in substrate-like behavior and inactivation of the serpin. It was found that neutrophil elastase cleaves C1-inh at sites of inflammation *in vivo* (56). Since RCL insertion increases heparin affinity (Fig. 4), it can be hypothesized that RCL-cleaved C1-inh is preferably recruited to the endothelial wall lined with GAGs. This may explain the puzzling observations of Liu *et al.* (6), who noticed that cleaved C1-inh possesses higher anti-inflammatory activity (not mediated through proteinase inhibition) under certain conditions than active C1-inh. Charge distribution of latent rC1-inh (Fig. 5*A*) explains the increased heparin affinity of both the latent and the similar cleaved C1-inh, since the positive surface patch on the "top" becomes more accessible after RCL insertion.

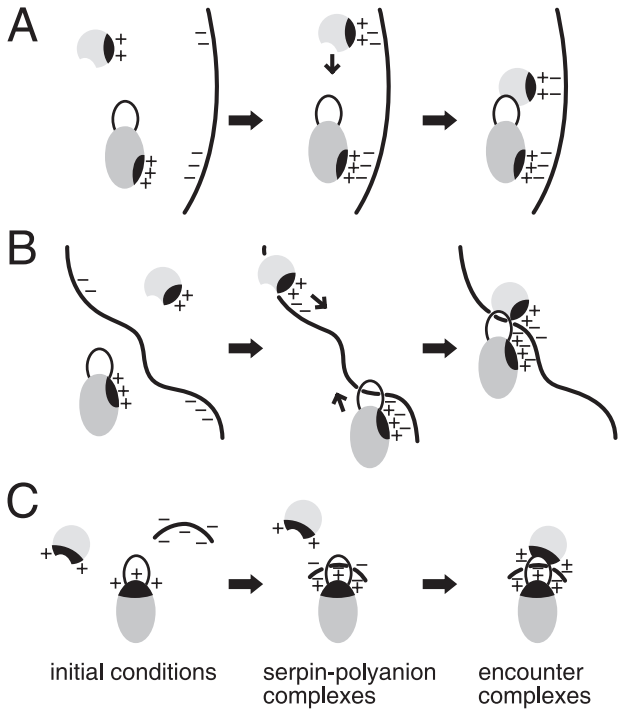

FIGURE 7. **Different mechanisms of the polyanion potentiation of serpins.** Serpins are shown as *ellipses*, proteinases as *circles*, and polyanions as *lines* in this schematic representation. Charged binding regions on proteins are marked with *black* and *charge signs*. *A*, the most prominent type of serpin activation by the "bridging" mechanism is depicted (19, 20). Antithrombin binds tightly to a specific site on the heparin chain. Thrombin binds to the same chain, but with lower affinity. Only thrombin diffuses one-dimensionally toward antithrombin until the encounter. Even then, they bind to different segments on heparin. *B*, the similar "co-occupation" mechanism proposed for protein C inhibitor is shown (29). Protein C inhibitor and protein C bind to the same polyanion chain, but neither binds with high affinity. Both proteins migrate along the chain until the encounter. In the Michaelis complex, they bind to the same site on the polyanion. *C*, the "sandwich" mechanism is shown. C1-inh binds a short polyanion with low affinity. Binding neutralizes surface charge at a specific region. Proteinase is now attracted to this surface, which happens to be the contact site in the encounter complex.

Structures of serpin-proteinase encounter complexes show extended interactions between the serpin and the proteinase besides the RCL (19–22). In addition, GAGs can accelerate certain reactions up to 1000-fold under physiological conditions. The different types of interaction with heparin and related polyanions are depicted in Fig. 7. It was shown earlier that effective complement inhibition is achieved by heparin through C1-inh in blood plasma (17). *In vivo* studies in rats also showed the effectiveness of polyanions via C1-inh (57). The potentiation effect was also demonstrated on the C1 complex (58) and on its isolated components C1r and C1s (47). The presence of a single major positively charged region in the contact surface of C1-inh (Fig. 5, *A* and *B*) led us to consider the simplest sufficient mechanism of GAG potentiation of C1-inh, charge neutralization. The proposed "sandwich" mechanism (Fig. 7) can account for at least five issues in the literature: (i) heparin and other polyanions increase C1-inh activity toward proteases with a basic surface near the substrate binding site and decrease it toward ones with an acidic surface; (ii) increased polyanion charge density magnifies both the potentiatory and hindering effect (45, 46, 48); (iii) low dependence on polyanion chain length (18, 46); (iv) absence of allosteric change upon polyanion

addition (18); and (v) neutralization of the fXIa surface alone leads to increased rate of inhibition (59). C1-inh activity is influenced to a varying degree by GAGs toward different proteases. The surface charge at the binding site of the above mentioned proteinases (Fig. 5*B*) correlates excellently with the observed effect. For instance, the potentiation factor of GAGs is the highest for the reaction with fXIa, which carries the most positive charges. In addition, dextran sulfate, which has the highest negative charge density, has the highest impact on C1-inh activity. The observation that the potentiation effect of short-chain polyanions is nearly as high as that of long-chain polyanions indicates that bridging does not play an important role in the case of C1-inh. Finally, a study on fXIa demonstrated that mutating basic residues to alanine in the so-called autolysis loop improved C1-inh activity toward the mutant enzyme by ~15-fold (59). Neutralizing the contact surface hence mimics the effect of polyanions. It must be noted that the portrayed mechanisms are not mutually exclusive. Heparin affinity of individual serpin and proteinase components determine the contribution of neutralization and bridging. C1-inh has the lowest affinity to heparin among the mentioned serpins (Fig. 7). The lifetime of the C1-inh-polyanion complex (57) is possibly too short for a bridging mechanism to be effective; only in the case of fXIa can a small template effect be observed (60).

Overall, the proposed model, which we call a "sandwich" mechanism, represents the simplest mechanism that explains the published data. Our results also illustrate that despite the so far observed strict conservation of the C terminus, interactions that stabilize the active metastable form can differ substantially among serpins. The structure opens up the possibility to characterize the interaction of plasma and extracellular matrix proteins with C1-inh at the atomic level. Based on the results obtained from this study, rational design of C1-inh variants with enhanced therapeutic potential is now feasible.

Acknowledgments—We thank Bálint Kupcsulik, Dávid Domonkos, and Kálmán Könczöl for useful discussions and experimentation regarding Pichia expression. We gratefully thank Santosh Panjikar for assistance in using the beamline X11 (EMBL outstation at DESY, Hamburg, Germany). The excellent staff support of the beamline is acknowledged.

REFERENCES

1. Gettins, P. G. W. (2002) *Chem. Rev.* **102,** 4751–4803
2. Huntington, J. A., Read, R. J., and Carrell, R. W. (2000) *Nature* **407,** 923–926
3. Dementiev, A., Dobó, J., and Gettins, P. G. W. (2006) *J. Biol. Chem.* **281,** 3452–3457
4. Bos, I. G. A., Hack, C. E., and Abrahams, J. P. (2002) *Immunobiology* **205,** 518–533
5. Jiang, H., Wagner, E., Zhang, H., and Frank, M. M. (2001) *J. Exp. Med.* **194,** 1609–1616
6. Liu, D., Cai, S., Gu, X., Scafidi, J., Wu, X., and Davis, A. E., III (2003) *J. Immunol.* **171,** 2594–2601
7. Cai, S., and Davis, A. E., 3rd. (2003) *J. Immunol.* **171,** 4786–4791
8. Odermatt, E., Berger, H., and Sano, Y. (1981) *FEBS Lett.* **131,** 283–285
9. Bock, S. C., Skriver, K., Nielsen, E., Thøgersen, H.-C., Wiman, B., Donaldson, V. H., Eddy, R. L., Marrinan, J., Radziejewska, E., Huber, R., Shows, T. B., and Magnusson, S. (1986) *Biochemistry* **25,** 4292–4301
10. Perkins, S. J., Smith, K. F., Amatayakul, S., Ashford, D., Rademacher, T. W., Dwek, R. A., Lachmann, P. J., and Harrison, R. A. (1990) *J. Mol. Biol.* **214,** 751–763
11. Coutinho, M., Aulak, K. S., and Davis, A. E., III (1994) *J. Immunol.* **153,** 3648–3654
12. Bos, I. G. A., Lubbers, Y. T. P., Roem, D., Abrahams, J. P., Hack, C. E., and Eldering, E. (2003) *J. Biol. Chem.* **278,** 29463–29470
13. Bowen, T., Cicardi, M., Farkas, H., Bork, K., Kreuz, W., Zingale, L., Varga, L., Martinez-Saguer, I., Aygören-Pürsün, E., Binkley, K., Zuraw, B., Davis, A., III, Hebert, J., Ritchie, B., Burnham, J., Castaldo, A., Menendez, A., Nagy, I., Harmat, G., Bucher, C., Lacuesta, G., Issekutz, A., Warrington, R., Yang, W., Dean, J., Kanani, A., Stark, D., McCusker, C., Wagner, E., Rivard, G.-E., Leith, E., Tsai, E., MacSween, M., Lyanga, J., Serushago, B., Leznoff, A., Waserman, S., and de Serres, J. (2004) *J. Allergy Clin. Immunol.* **114,** 629–637
14. Gadek, J. E., Hosea, S. W., Gelfand, J. A., Santaella, M., Wickerhauser, M., Triantaphyllopoulos, D. C., and Frank, M. M. (1980) *N. Engl. J. Med.* **302,** 542–546
15. Caliezi, C., Wuillemin, W. A., Zeerleder, S., Redondo, M., Eisele, B., and Hack, C. E. (2000) *Pharmacol. Rev.* **52,** 91–112
16. van Doorn, M. B. A., Burggraaf, J., van Dam, T., Eerenberg, A., Levi, M., Hack, C. E., Schoemaker, R. C., Cohen, A. F., and Nuijens, J. (2005) *J. Allergy Clin. Immunol.* **116,** 876–883
17. Caughman, G. B., Boackle, R. J., and Vesely, J. (1982) *Mol. Immunol.* **19,** 287–295
18. Bos, I. G. A. C. (2003) *C1-Inhibitor potentiation by glycosaminoglycans*, CIP-Gegevens Koninklijke Bibliotheek, The Hague, Netherlands
19. Li, W., Johnson, D. J. D., Esmon, C. T., and Huntington, J. A. (2004) *Nat. Struct. Mol. Biol.* **11,** 857–862
20. Dementiev, A., Petitou, M., Herbert, J.-M., and Gettins, P. G. W. (2004) *Nat. Struct. Mol. Biol.* **11,** 863–867
21. Johnson, D. J. D., Li, W., Adams, T. E., and Huntington, J. A. (2006) *EMBO J.* **25,** 2029–2037
22. Baglin, T. P., Carrell, R. W., Church, F. C., Esmon, C. T., and Huntington, J. A. (2002) *Proc. Natl. Acad. Sci. U. S. A.* **99,** 11079–11084
23. Kabsch, W. (1993) *J. Appl. Crystallogr.* **26,** 795–800
24. Collaborative Computational Project 4 (1994) *Acta Crystallogr. Sect. D* **50,** 760–763
25. Guex, N., and Peitsch, M. C. (1997) *Electrophoresis* **18,** 2714–2723
26. Murshudov, G. N., Vagin, A. A., and Dodson, E. J. (1997) *Acta Crystallogr. Sect. D* **53,** 240–255
27. Emsley, P., and Cowtan, K. (2004) *Acta Crystallogr. Sect. D* **60,** 2126–2132
28. Im, H., Woo, M.-S., Hwang, K. Y., and Yu, M.-H. (2002) *J. Biol. Chem.* **277,** 46347–46354
29. Huntington, J. A., Kjellberg, M., and Stenflo, J. (2003) *Structure* **11,** 205–215
30. Skinner, R., Abrahams, J. P., Whisstock, J. C., Lesk, A. M., Carrell, R. W., and Wardell, M. R. (1997) *J. Mol. Biol.* **266,** 601–609
31. Jin, L., Pandey, P., Babine, R. E., Gorga, J. C., Seidl, K. J., Gelfand, E., Weaver, D. T., Abdel-Meguid, S. S., and Strickler, J. E. (2005) *J. Biol. Chem.* **280,** 4704–4712
32. Gaboriaud, C., Rossi, V., Bally, I., Arlaud, G. J., and Fontecilla-Camps, J. C. (2000) *EMBO J.* **19,** 1755–1765
33. Tang, J., Yu, C. L., Williams, S. R., Springman, E., Jeffery, D., Sprengeler, P. A., Estevez, A., Sampang, J., Shrader, W., Spencer J., Young, W., McGrath, M., and Katz, B. A. (2005) *J. Biol. Chem.* **280,** 41077–41089
34. Harmat, V., Gál, P., Kardos, J., Szilágyi, K., Ambrus, G., Végh, B., Náray-Szabó, G., and Závodszky, P. (2004) *J. Mol. Biol.* **342,** 1533–1546
35. Budayova-Spano, M., Grabarse, W., Thielens, N. M., Hillen, H., Lacroix, M., Schmidt, M., Fontecilla-Camps, J. C., Arlaud, G. J., and Gaboriaud, C. (2002) *Structure* **10,** 1509–1519
36. Bohne-Lang, A., and von der Lieth, C.-W. (2005) *Nucleic Acids Res.* **33,** W214–W219
37. Baker, N. A., Sept, D., Joseph, S., Holst, M. J., and McCammon, J. A. (2001) *Proc. Natl. Acad. Sci. U. S. A.* **98,** 10037–10041
38. Krissinel, E., and Henrick, K. (2005) in *Computational Life Sciences, First International Symposium, CompLife 2005 Konstanz, Germany, September 25–27, 2005 Proceedings* (Berthold, M. R., Glen, R., Diederichs, K., Kohlbacher, O., and Fischer, I., eds) pp. 163–174, Springer-Verlag Berlin, Hei-

delberg, Germany
39. Jin, L., Abrahams, J. P., Skinner, R., Petitou, M., Pike, R. N., and Carrell, R. W. (1997) *Proc. Natl. Acad. Sci. U. S. A.* **94,** 14683–14688
40. Morris, G. M., Goodsell, D. S., Halliday, R. S., Huey, R., Hart, W. E., Belew, R. K., and Olson, A. J. (1998) *J. Comput. Chem.* **19,** 1639–1662
41. Mottonen, J., Strand, A., Symersky, J., Sweet, R. M., Danley, D. E., Geoghegan, K. F., Gerard, R. D., and Goldsmith, E. J. (1992) *Nature* **355,** 270–273
42. Carrell, R. W., Stein, P. E., Fermi, G., and Wardell, M. R. (1994) *Structure* **2,** 257–270
43. Irving, J. A., Pike, R. N., Lesk, A. M., and Whisstock, J. C. (2000) *Genome Res.* **10,** 1845–1864
44. Patston, P. A., Hauert, J., Michaud, M., and Schapira, M. (1995) *FEBS Lett.* **368,** 401–404
45. Wuillemin, W. A., Eldering, E., Citarella, F., de Ruig, C. P., ten Cate, H., and Hack, C. E. (1996) *J. Biol. Chem.* **271,** 12913–12918
46. Mauron, T., Lämmle, B., and Wuillemin, W. A. (1998) *Thromb. Haemost.* **80,** 82–86
47. Sim, R. B., Arlaud, G. J., and Colomb, M. G. (1980) *Biochim. Biophys. Acta* **612,** 433–449
48. Wuillemin, W. A., te Velthuis, H., Lubbers, Y. T. P., de Ruig, C. P., Eldering, E., and Hack, C. E. (1997) *J. Immunol.* **159,** 1953–1960
49. Gozzo, A. J., Nunes, V. A., Nader, H. B., Dietrich, C. P., Carmona, A. K., Sampaio, M. U., Sampaio, C. A. M., and Araújo, M. S. (2003) *Braz. J. Med. Biol. Res.* **36,** 1055–1059
50. Eldering, E., Verpy, E., Roem, D., Meo, T., and Tosi, M. (1995) *J. Biol. Chem.* **270,** 2579–2587
51. Aulak, K. S., Eldering, E., Hack, C. E., Lubbers, Y. P. T., Harrison, R. A., Mast, A., Cicardi, M., and Davis, A. E., III (1993) *J. Biol. Chem.* **268,** 18088–18094
52. Kalmár, L., Hegedüs, T., Farkas, H., Nagy, M., and Tordai, A. (2005) *Hum. Mutat.* **25,** 1–5
53. Cumming, S.-A., Halsall, D. J., Ewan, P. W., and Lomas, D. A. (2003) *J. Med. Genet.* **40,** e114
54. Zhou, A., Huntington, J. A., and Carrell, R. W. (1999) *Blood* **94,** 3388–3396
55. Zahedi, R., MacFarlane, R. C., Wisnieski, J. J., and Davis, A. E., III (2001) *J. Immunol.* **167,** 1500–1506
56. Nuijens, J. H., Eerenberg-Belmer, A. J. M., Huijbregts, C. C. M., Schreuder, W. O., Felt-Bersma, R. J. F., Abbink, J. J., Thijs, L. G., and Hack, C. E. (1989) *J. Clin. Invest.* **84,** 443–450
57. Bos, I. G. A. C., van Mierlo, G. J., Bleeker, W. K., Rigter, G. M. M., te Velthuis, H., Dickneite, G., and Hack, C. E. (2001) *Int. Immunopharmacol.* **1,** 1583–1595
58. Caldwell, E .E. O., Andreasen, A. M., Blietz, M. A., Serrahn, J. N., Vander-Noot, V., Park, Y., Yu, G., Linhardt, R. J., and and Weiler, J. M. (1999) *Arch. Biochem. Biophys.* **361,** 215–222
59. Rezaie, A. R., Sun, M.-F., and Gailani, D. (2006) *Biochemistry* **45,** 9427–9433
60. Zhao, M., Abdel-Razek, T., Sun, M.-F., and Gailani, D. (1998) *J. Biol. Chem.* **273,** 31153–31159